Science Advances
AAAS

Supplementary Materials for

Hox genes control homocercal caudal fin development and evolution

Nicolás Cumplido *et al.*

Corresponding author: Nicolás Cumplido, nicump@gmail.com

Sci. Adv. **10**, eadj5991 (2024)
DOI: 10.1126/sciadv.adj5991

The PDF file includes:

Other Supplementary Material for this manuscript includes the following:

Supplementary Text

Expression patterns of zebrafish *hox13* genes

Tail. —At 1 dpf, all six *hox13* paralogs were expressed in the tail bud, with varying anterior limits of expression. The *hoxc* paralogs *c13a* and *c13b*, had the broadest expression domains, which extended more anteriorly. Particularly, *c13a* expression extended into the fin fold. The *hoxa* and *b* paralogs, *a13a*, *a13b* and *b13a*, showed similar and more posterior expression domains, while the *hoxd* paralog, *hoxd13a*, was confined to the posterior tip of the tail.

At 2 dpf, all *hox13* genes, except for *d13a*, were expressed in the tail with distinct expression patterns either in the mesenchyme around the notochord, the fin fold and/or the neural tube (Fig. S1). The *hoxc* paralogs had broader expression domains that overlapped both *hoxa* paralogs and the *b13a* gene expression, while the expression patterns of *hoxa* paralogs versus *b13a* did not overlap and were confined to either the anterior or posterior portion of the tail, respectively (Fig. S1). Overall, the *b13a*, *c13a*, and *c13b* paralogs had strong labeling in the tail, while the expression of *a13a* and *a13b* paralogs was considerably fainter compared to their expression in the pectoral buds.

By 3 dpf, expression of only the *a13b*, *b13a*, *c13a* and *c13b* genes was detected in the tail, with varying expression domains (Fig. S2). In the ventroposterior portion of the notochord, *a13b* had the most anterior expression, followed by *hoxc* paralogs and then *b13a*. Dorsally, the most anterior domain was observed in *hoxc* paralogs, followed by *b13a* and *a13b*. At 4 dpf, *a13b*, *b13a* and *c13a* genes were detected, with the expression of *a13b* much fainter compared to its expression in the pectoral fins. Additionally, when considering the PU/U boundary (black arrow, Fig. S2) ventral expression of *a13b* was located at the PU/U boundary, while *c13a* was also expressed at this boundary but reaching almost the middle portion of the ural region. Conversely, *b13a* was expressed in the posterior end of the ural region. Dorsally, all these genes were expressed in the preural region, with the *b13a* gene expressed also in the dorsal portion of the ural region.

Between 1 and 3 dpf, the expression patterns of the two *hoxc13* ohnologs, *c13a* and *c13b* were highly similar, but *c13a* expression persisted longer than *c13b* expression (Figs. S1, S2), as previously reported (*26*).

Pectoral fins. —Consistent with previous studies (*32, 34*), we detected expression of *hoxa* and *hoxd* paralogs in the pectoral fin at 2, 3 and 4 dpf. At 2 dpf, these genes were expressed at the distal mesenchyme of the pectoral fin bud, with *d13a* expression confined to its posterior region (Fig. S1). At 3 dpf, *a13a* lost its proximal mesenchymal expression, and instead was expressed only in the distal fin fold (*34*), resembling the pattern observed in the posterior portion of the tail between 1 and 2 dpf (Fig. S1). We did not detect expression of *b13a* or any of the *hoxc* paralogs in the pectoral fin at any time point.

Proctodeum/Cloaca. —The proctodeum or embryonic cloaca is an ectodermal derivative that invaginates and fuses with the hindgut to form the anus. As previously reported, *a13b* (*96*) and *d13a* (*97*) were expressed in this region, as well as *a13a*, suggesting a *hoxa/d* expression pattern in this tissue. Similar to the tail and pectoral fin, *d13a* expression was located more posteriorly than other *hox13* paralogues.

Pronephric duct. —The pronephric duct is a component of the embryonic urogenital duct that arises from the lateral plate mesoderm. It consists of two bilateral ducts located dorso-lateral to the gut, which eventually terminate at the urogenital pore. Previous studies have shown that *a13b* is expressed in this region (*96*), and our findings confirm this expression from 1– to 4–dpf (Figs. S1, S2A). We also observed the expression of *c13b* in the same region, which persisted from 1 to 3 dpf (Figs. S1, S2A).

1.5 Hindgut. — The hindgut is the most posterior section of the digestive tract that fuses during embryonic development with the proctodeum, creating a functional gastrointestinal tube. Previous studies in zebrafish have only reported the expression of *a13a* in this region (*96*). We observed *a13a* expression in the most posterior portion of the hindgut at 1 dpf. Additionally, we report a previously unobserved expression of *c13a* in this region, extending further anteriorly (Fig. S1). Between 2 and 4 dpf, we observed strong *in situ* labeling of *a13a*, *b13a* and *c13a* in the hindgut, with transient inclusion of *a13b* at 3 dpf (Fig. S2A). Hence, the *hoxa*, *b* and *c* expressions in the hindgut resembled the activation of the same genes during tail development (Fig. S2).

2. List of characters, their coding, and comments

Character 1. Number of preural vertebrae: more than six [0]; six or less [1].

Comments—Original character.

Character 2. Ural region in adults including: more than two ural centra (polyural condition) [0]; commonly two (or less) ural centra (diural condition) [1]

Comments—The diural caudal skeleton was proposed as a synapomorphy of teleosts by Patterson (*98*). For further explanation on this character and the homology problems involved see Schultze and Arratia (*4, 7, 73*), Wiley et al. (*82*) and Cumplido et al. (*40*). Character 127 in Arratia (*45*) and 147 in Arratia (*44*).

Character 3. Ural neural arches modified as uroneurals: ural neural arches unmodified [0]; all or some of the last ural neural arches modified as uroneurals [1]

Comments—Modified from Arratia (*43*). This character has been consistently used in systematic studies of teleosts. See for instance: Patterson (*42, 98*), Brito (*99*), Grande and Bemis (*71*), Schultze and Arratia (*4, 7, 73, 100*), Arratia and Schultze (*74*), and Arratia (*43, 45, 101–103*). Character 132 in Arratia (*45*) and 152 in Arratia (*44*).

Character 4. Preural vertebrae 3 of adult individuals: with haemal arches autogenous or articulating with the centrum [0]; fused with the centrum [1].

Comments—Modified from Arratia (*43*), which also included the preural vertebrae 2. Character 121 in Arratia (*45*) and 141 in Arratia (*44*).

Character 5. Neural spine of preural centrum 1: long, close or extending to the dorsal margin of the body [0]; short or absent [1].

Comments—From Arratia (*43*). Character 123 in Arratia (*45*) and 143 in Arratia (*44*).

Character 6. Number of principal caudal rays: fewer than 19 [0]; 20 to 30 [1]; 19 [2]; more than 40 rays [3].

Comments—Modified from Patterson (*98*), Patterson and Rosen (*104*), and Arratia (*44, 45, 101*). Character 148 in Arratia (*45*) and 173 in Arratia (*44*).

Character 7. Hypurals 2 and 3: without a space between them [0]; with a space (hypural diastema) between them; non-applicable, e.g., fusion of hypurals [–].

Comments—From Arratia (*43*). Character 141 in Arratia (*45*) and 161 in Arratia (*44*).

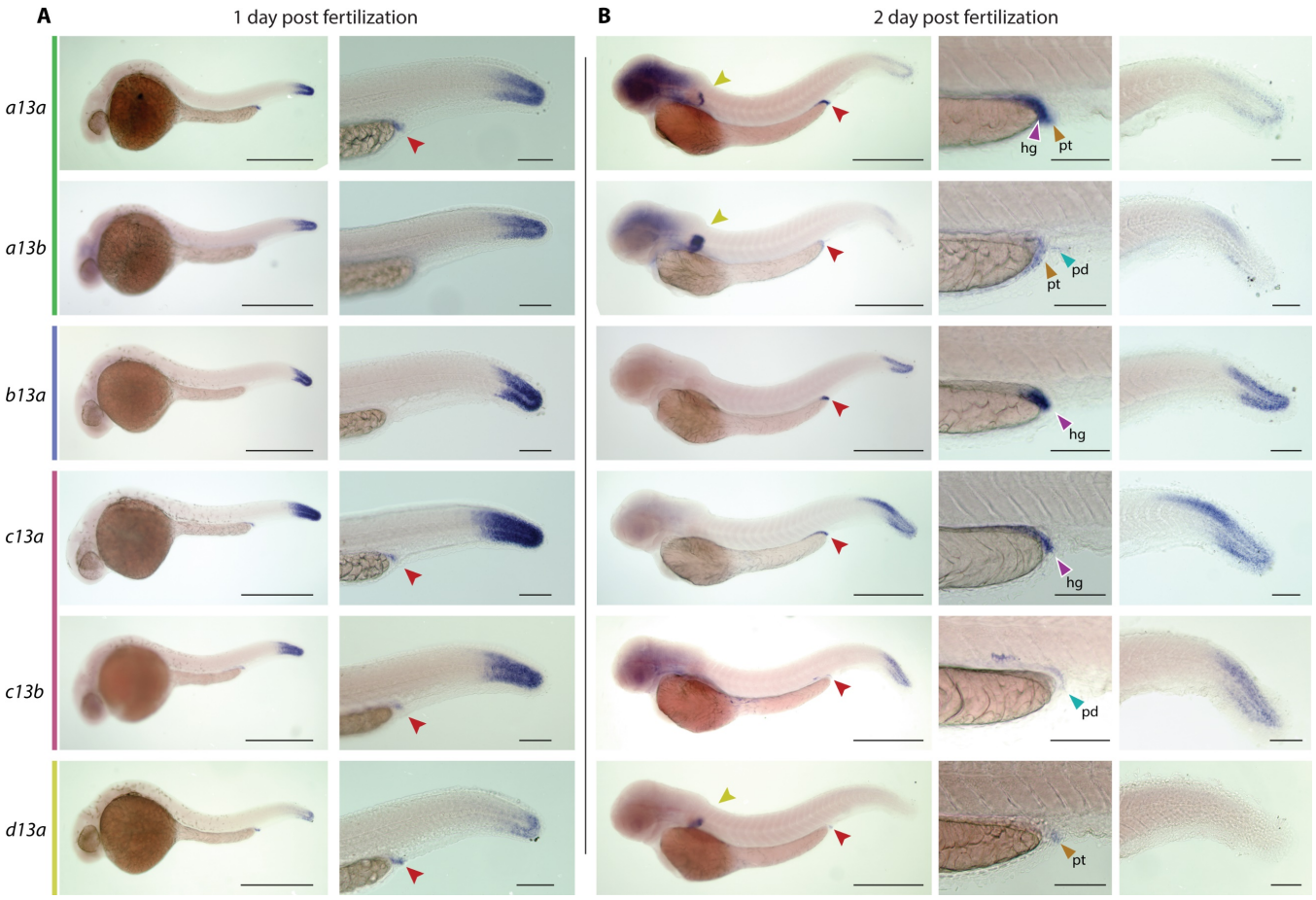

Fig. S1. Gene expression patterns of zebrafish *hox13* paralogs at 1 and 2 dpf. *In situ* hybridizations were performed against *a13a*, *a13b*, *b13a, c13a, c13b,* and *d13a* to visualize their expression patterns. (**A**), 1 dpf zebrafish larvae. Left panels, whole larvae in lateral view, scale bar at 0.5 mm. Right panels provide a close-up of the tail, scale bar at 0.1 mm. (**B**), 2 dpf zebrafish larvae. Left panels, whole larvae in lateral view, scale bar at 0.5 mm. Middle panels close-up to the anus, right panels close-up to the tail. Middle and right panel scale bars at 0.1 mm. For **A, B**, The yellow arrowhead points at the expression in the pectoral fins, the red arrowhead at the posterior end of either the hindgut (hg, purple arrowhead), pronephric duct (pd, light blue arrowhead), or proctodeum/cloaca (pt, orange arrowhead).

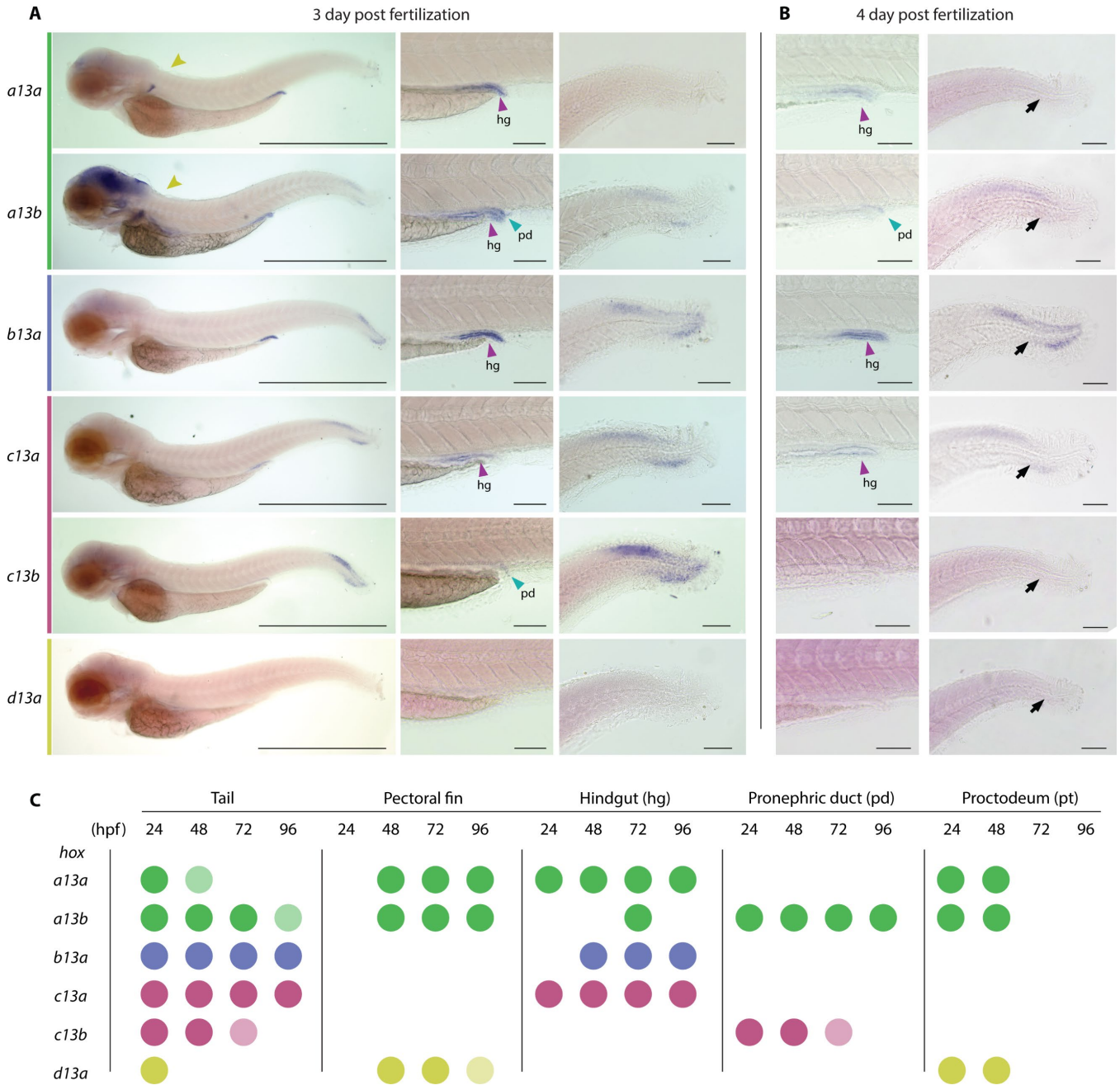

Fig. S2. Gene expression patterns of *hox13* zebrafish paralogs at 3 and 4 dpf. *In situ* hybridizations were performed against *a13a*, *a13b*, *b13a, c13a, c13b,* and *d13a* at 3 and 4 dpf to visualize their expression patterns. (**A**), 3 dpf zebrafish larvae. Left panels show larvae in lateral view, scale bar at 0.5 mm. Middle panels provide a close-up to the anus, scale bar at 0.1 mm. Right panels provide a close-up to the tail, scale bar at 0.1 mm. (**B**), 4 dpf zebrafish larvae. Left panels provide a close-up to the anus, scale bar at 0.1 mm. Right panels provide a close-up to the tail, scale bar at 0.1 mm. For **A**, **B**, yellow arrowheads point at the expression in the pectoral fins, purple arrowheads highlight at the expression in the hindgut (hg), and light blue arrowheads show *hox* gene expression in the pronephric duct (pd). Black

arrows indicate the position of the end of the caudal artery that delimits the position of the PU/U boundary. (**C**), Summary of the expression patterns of all *hox13* paralogs in different tissues over time.

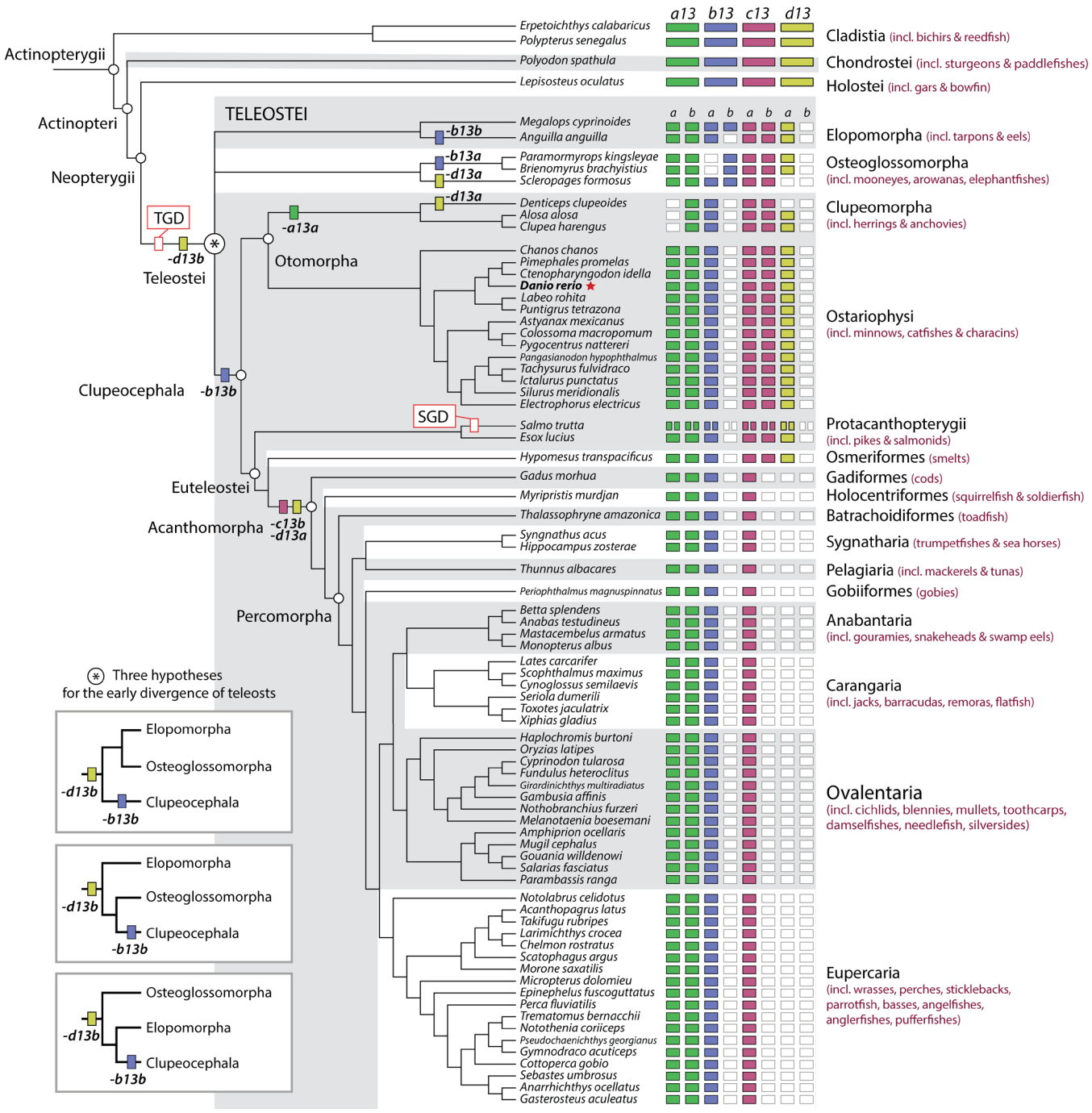

Fig. S3. Reconstruction of *hox13* gene repertoire evolution in actinopterygians. The presence vs absence of each *hox13* gene was determined by manually searching for each *Hox* cluster in annotated genome assemblies of actinopterygians available on NCBI (see Table S1). The simplified phylogeny is based on Betancur-R et al. (*105*), with the base of the teleosts resolved as a polytomy. Boxed, at the bottom left of the figure, are the three possible scenarios of the most basally diverging group, including Elopomorpha (*105*), Osteoglossomorpha (*98*) or Clupeocephala (*106*) although these do not affect the interpretations of *hox13* gene evolution. The presence of each gene is indicated by a coloured rectangle, green for *hoxa13*, blue for *hoxb13*, red for *hoxc13*, and yellow for *hoxd13* orthologs. Empty (white)

rectangles indicate the absence of the respective gene. Zebrafish (*Danio rerio*) is in bold and indicated with a red star. TGD, teleost genome duplication; SGD, salmonid genome duplication.

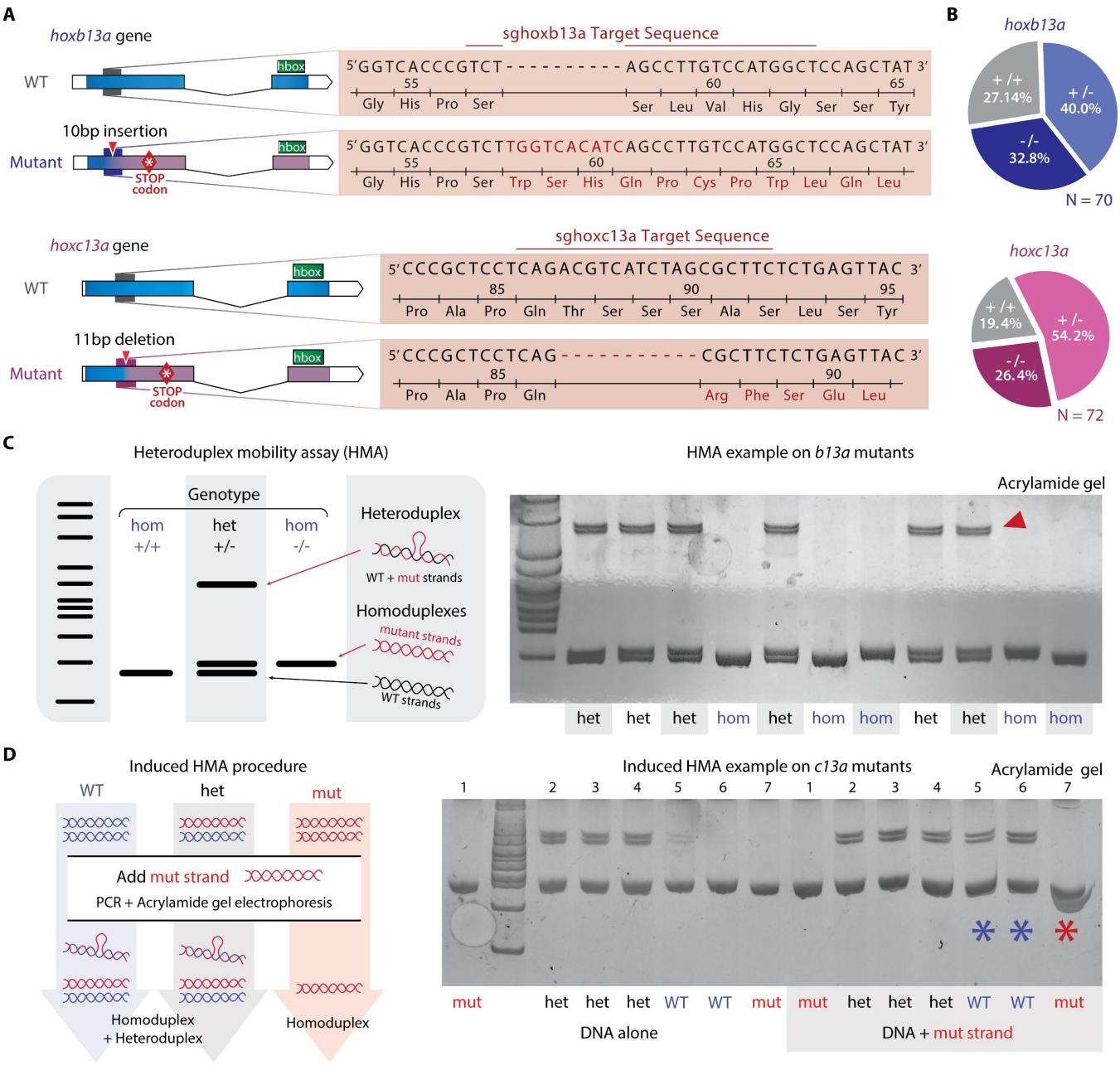

Fig. S4. Description of *b13a* and *c13a* gene mutations and genotyping procedure. (**A**), Description of the 10bp insertion mutation in *b13a* and the 11-bp deletion in *c13a* genes, both of which were generated using CRISPR/Cas9. Both mutations cause a frameshift in the first exon resulting in an early stop codon. The DNA binding homeobox (hbox) is encoded by the second exon in both genes. (**B**), An incross of heterozygous *b13a* and *c13a* mutant zebrafish, produced a mendelian ratio of inheritance for the more than 70 F2 individuals tested. (**C**), Genotyping of both clutches was performed using a heteroduplex mobility assay. In this assay, the presence of strands of different sizes in heterozygous fish leads to the formation of a heteroduplex, which delays DNA migration during acrylamide gel electrophoresis (red arrowhead). (**D**), Homozygous mutants were identified by adding homozygous mutant DNA to each unknown sample. If the unknown sample was from a wild type or heterozygous individual, the presence of the mutant DNA would cause a heteroduplex mobility shift, which could be

detected by the presence of a delayed band in the acrylamide gel (blue asterisk). Homozygous mutant samples, on the other hand, would not generate this band, and were identified by the absence of the delayed band (red asterisk).

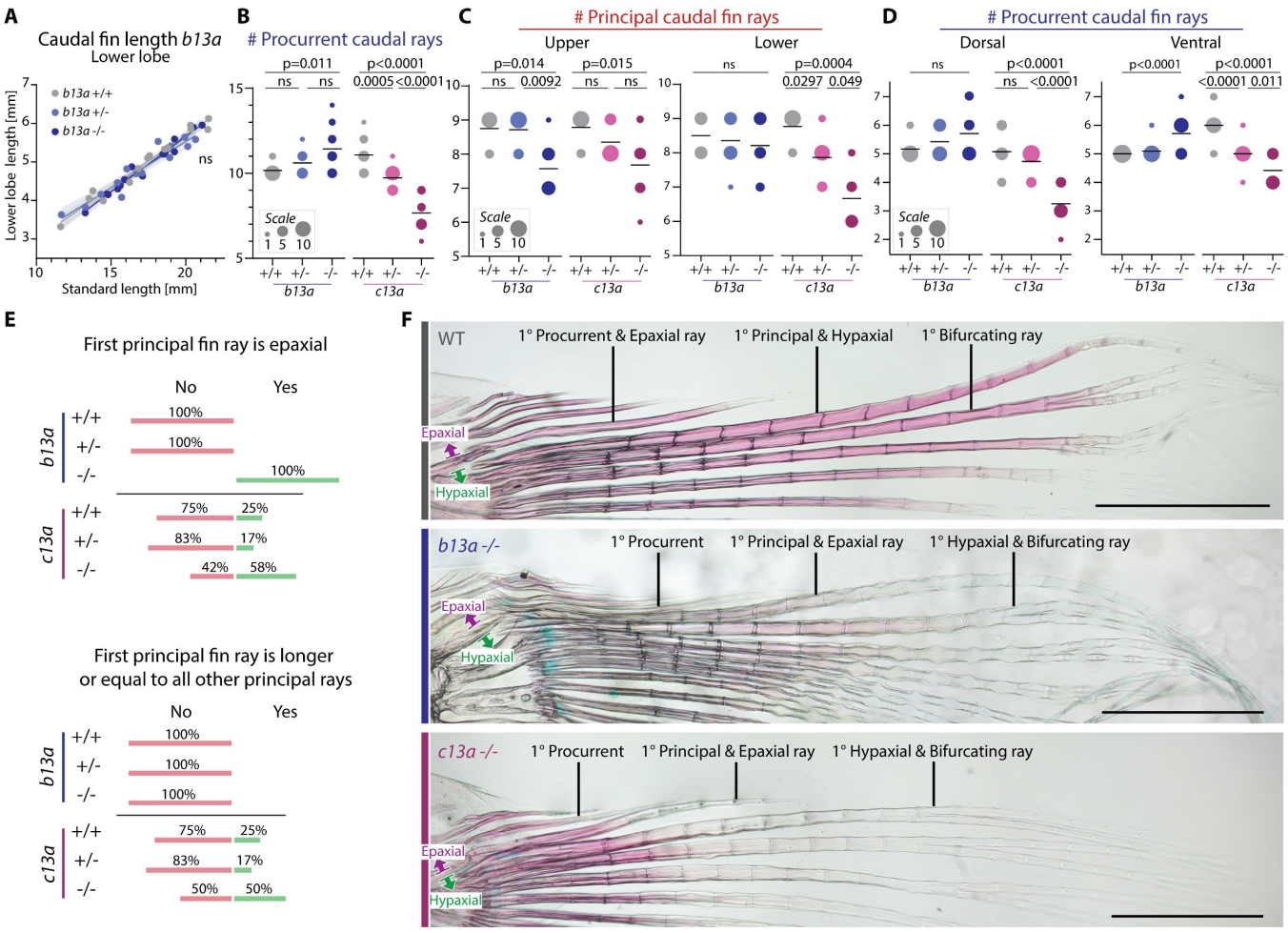

Fig. S5. Quantification of caudal fin phenotypes in *b13a* and *c13a* mutants. (**A**), Lower lobe length relative to standard length in wild-type, heterozygous and homozygous *b13a* mutant siblings (*n*=14). ANCOVA indicated no variation in lower lobe length between genotypes ($F_{(2,38)}$=1.076, p=0.3510). Shaded area represents the 95% confidence interval around the regression line. For B–E, *n*= $b13a^{+/+}$:12, $b13a^{+/-}$:14, $b13a^{-/-}$:14, $c13a^{+/+}$:13, $c13a^{+/-}$:15 and $c13a^{-/-}$:12. Each graph presents the mean, and the circle size is proportional to the number of individuals. (**B**), Procurrent ray number in both mutants. Poisson regressions revealed significant increases in procurrent ray number in *b13a* mutants ($\chi^2_{(2)}$=15.04, p=0.0005). ANOVA revealed significant reduction in procurrent ray number for *c13a* mutants ($F_{(2,37)}$=51.18, p<0.0001). Multiple comparisons indicated a *c13a* gene-dosage effect. (**C**), Principal ray number separated into upper and lower lobes in both mutants. Poisson regressions revealed a significant increase in upper principal ray number in *b13a* mutants ($\chi^2_{(2)}$=17.15, p<0.0001) but not in lower principal ray number ($\chi^2_{(2)}$=0.82, p=0.66). Poisson regressions revealed a significant reduction in both upper and lower lobes of *c13a* mutants (*upper*: $\chi^2_{(2)}$=10.95, p<0.0042; *lower*: $\chi^2_{(2)}$=25.40, p<0.0001). (**D**), Procurrent ray number separated into dorsal and ventral series in both mutants. Poisson regression revealed a significant increase in ventral procurrent rays in *b13a* mutants ($\chi^2_{(2)}$=14.75, p=0.0006) but not dorsal procurrent rays ($\chi^2_{(2)}$=4.68, p=0.089). ANOVA revealed a significant decrease in procurrent ray number in both upper and lower procurrent rays in *c13a* mutants (*upper*: $F_{(2,37)}$=30.81, p<0.0001; *lower*: $F_{(2,37)}$=33.58, p<0.0001). (**E**), Frequencies of the first principal ray being epaxial, or longer than other principal rays in both mutants. (**F**), Cleared and stained skeletal preparations

highlighting the first principal and dorsal procurrent fin rays. The first principal ray (in red) is the first non-bifurcating ray adjacent to a bifurcating ray. Epaxial rays (in purple) vs hypaxial rays (in green) refer to the relation between fin ray bases and the position of the notochord (1 mm scale bar).

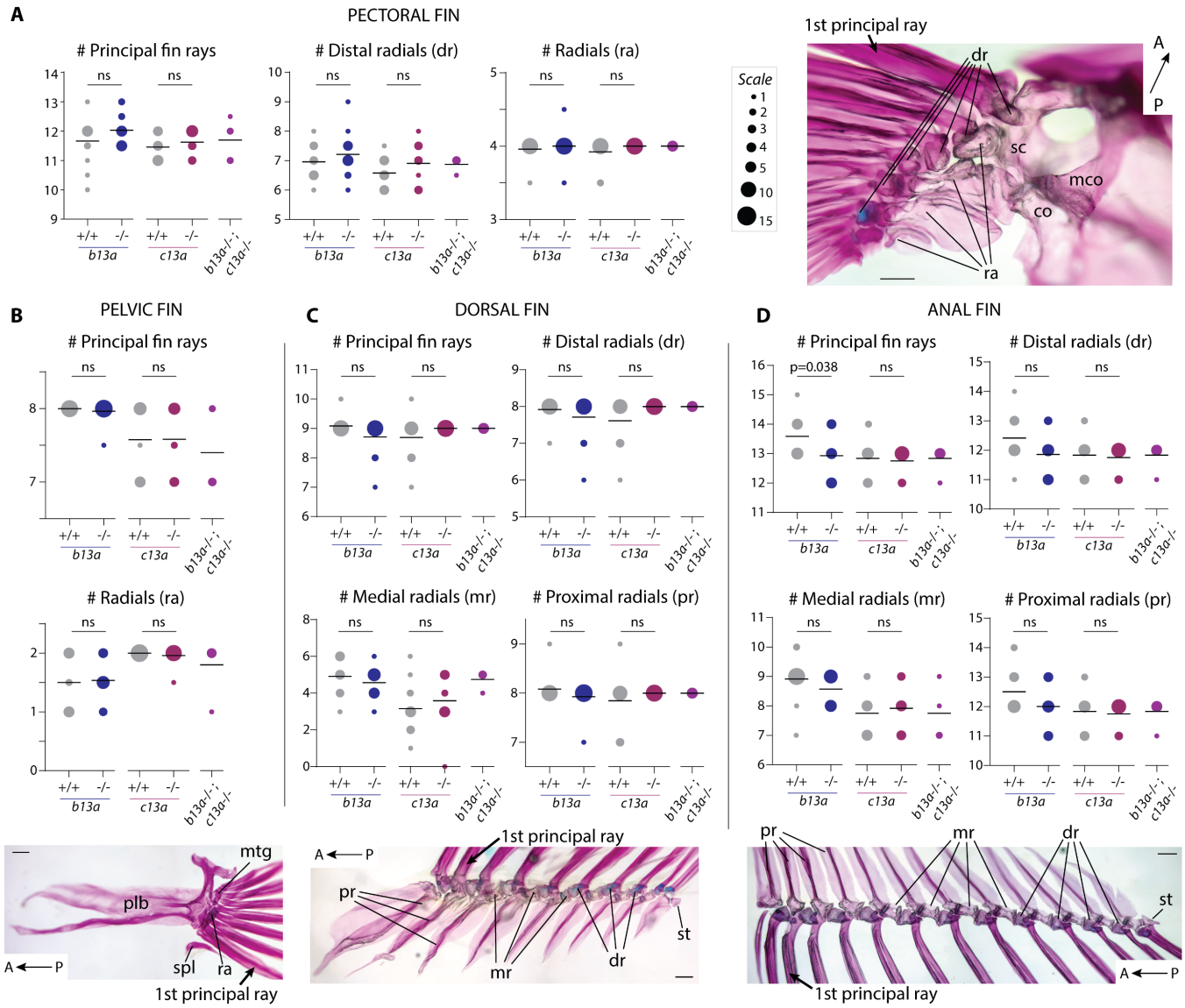

Fig. S6. Dorsal, anal, pectoral, and pelvic fin ray and radial counts in single and double *b13a*$^{-/-}$; *c13a*$^{-/-}$ zebrafish mutants. The number of principal fin rays and radials for the zebrafish fins, excluding the caudal fin, is shown (*n*= *b13a*$^{+/+}$:12, *b13a*$^{+/-}$:14, *b13a*$^{-/-}$:14, *c13a*$^{+/+}$:13, *c13a*$^{+/-}$:15 and *c13a*$^{-/-}$:12, *b13a*$^{-/-}$; *c13a*$^{-/-}$:5). For paired fins, the number of left and right rays and radials were added. (**A**) Pectoral fin: left side endoskeleton shown in a dorsal view. ANOVA revealed no significant count variations in principal fin rays (*b13a:* $F_{(1,24)}$=1.85, p=0.19; *c13a*: $F_{(1,23)}$=0.89, p=0.35), distal radials (*b13a:* $F_{(1,24)}$=0.96, p=0.34; *c13a*: $F_{(1,22)}$=1.85, p=0.19) and radials (*b13a:* $F_{(1,24)}$=0.37, p=0.55; *c13a*: $F_{(1,22)}$=1.85, p=0.19). (**B**) Pelvic fin: left side shown in a ventral view. ANOVA revealed no significant count variation in principal fin rays (*b13a:* $F_{(1,24)}$=0.85, p=0.37; *c13a*: $F_{(1,23)}$=0.0011, p=0.97) and radials (*b13a:* $F_{(1,24)}$=0.047, p=0.83; *c13a*: $F_{(1,23)}$=1.09, p=0.31). (**C**) Dorsal fin: lateral view of endoskeleton. ANOVA revealed no significant count variation in principal fin rays (*b13a:* $F_{(1,24)}$=3.66, p=0.068; *c13a*: $F_{(1,23)}$=2.01, p=0.17), distal radials (*b13a:* $F_{(1,24)}$=1.10, p=0.30; *c13a*: $F_{(1,23)}$=4.18, p=0.05), middle radials (*b13a:* $F_{(1,24)}$=1.01, p=0.33; *c13a*: $F_{(1,23)}$=0.59, p=0.45) and proximal radials (*b13a:* $F_{(1,24)}$=2.01, p=0.17; *c13a*: $F_{(1,23)}$=0.92, p=0.35). (**D**) Anal fin: lateral view of endoskeleton. ANOVA revealed a significant

reduction in principal fin ray counts for *b13a* mutants ($F_{(1,24)}$=4.80, p=0.038) but not in *c13a* mutants ($F_{(1,22)}$=0.12, p=0.74). No significant variations were found in anal fin distal radials (*b13a:* $F_{(1,24)}$=3.32, p=0.081; *c13a*: $F_{(1,22)}$=0.12, p=0.74), middle radials (*b13a:* $F_{(1,24)}$=1.78, p=0.19; *c13a*: $F_{(1,22)}$=0.28, p=0.60) and proximal radials (*b13a:* $F_{(1,24)}$=2.98, p=0.097; *c13a*: $F_{(1,22)}$=0.12, p=0.74). In all measurements, the mean of double mutant ray number was within the margins of normal variations. Each graph presents the mean, and the circle size is proportional to the number of individuals. “ns” indicates a non-significant ANOVA test. In each image, scale bar is 200 μm, and anteroposterior axis is indicated with an arrow. *Abbrev.*: co, coracoid; dr, distal radial; mco, mesocoracoid; mr, middle radial; mtg, metapterygium; plb, pelvic bone; pr, proximal radial; ra, radial; sc, scapula; spl, splint; st, stay.

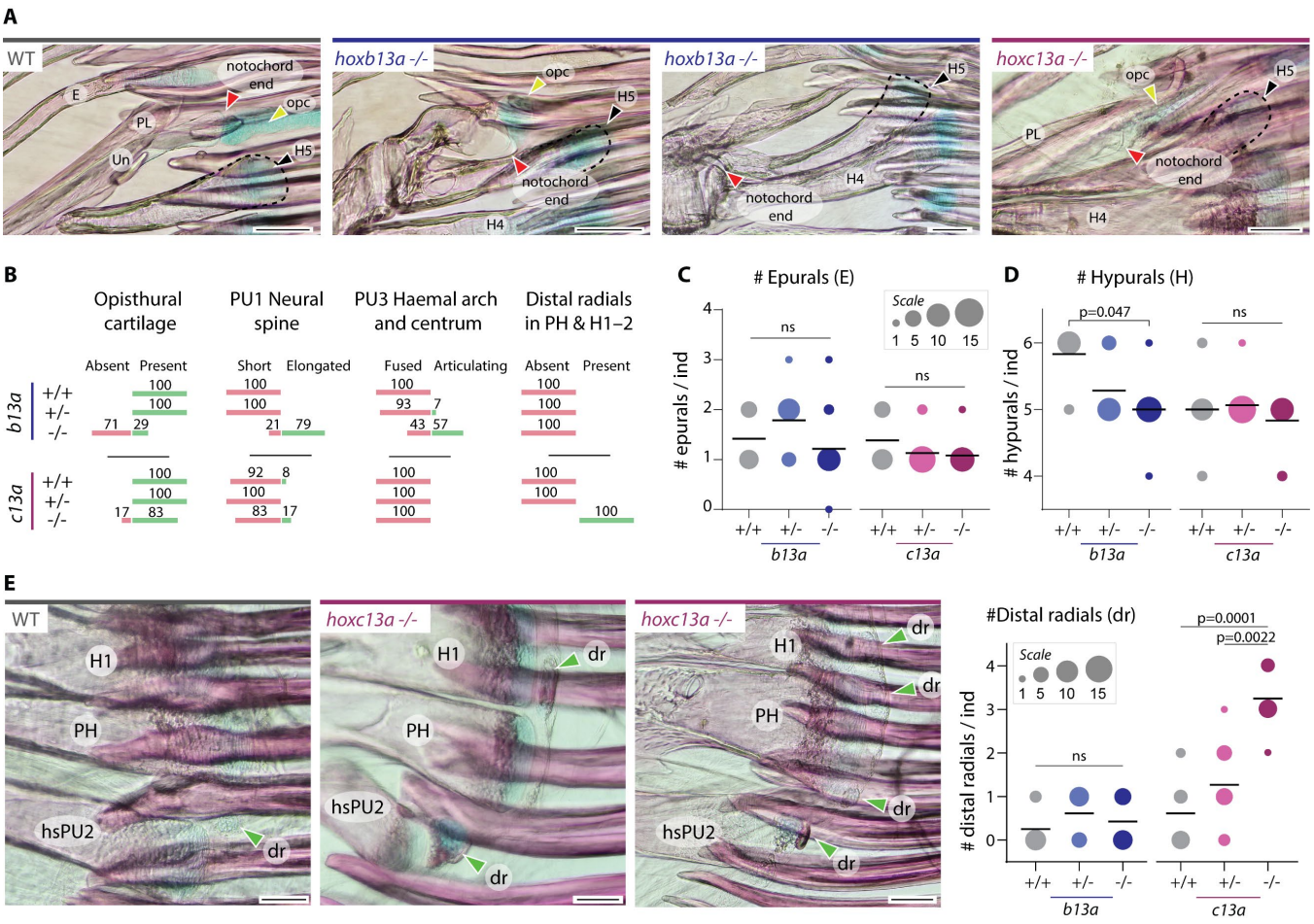

Fig. S7. Quantification of vertebral phenotypes in *b13a* and *c13a* mutants. (**A**), Relationship between the tip of the notochord (red arrowhead), the presence of an opisthural cartilage (yellow arrowhead) and the posterior end of the hypural 5 (dashed line with a black arrowhead). Both mutants exhibit an abbreviated notochord. For b–e, *n*= $b13a^{+/+}$:12, $b13a^{+/-}$:14, $b13a^{-/-}$:14, $c13a^{+/+}$:13, $c13a^{+/-}$:15 and $c13a^{-/-}$:12, $b13a^{-/-}$;$c13a^{-/-}$:4. (**B**), Frequencies for the presence of an opisthural cartilage, an elongated neural spine on the preural centrum 1, an articulating haemal arch on the preural centrum 3, and extra distal radials in *b13a* and *c13a* mutants. (**C**), Epural number for both mutants. Poisson regressions revealed no significant changes in epural number in both mutants (*b13a*: $\chi^2_{(2)}$=1.57, p=0.46; *c13a*: $\chi^2_{(2)}$=0.55, p=0.76). (**D**), Hypural number for both mutants. Poisson regressions revealed a significant decrease in hypural number in *b13a* mutants ($\chi^2_{(2)}$=8.50, p=0.014) but not in *c13a* mutants ($\chi^2_{(2)}$=1.05, p=0.36). Post-hoc comparisons showed a significant effect in $b13a^{-/-}$ mutants only. (**E**), Cleared and stained skeletal preparations showing the presence of extra distal radials, either cartilaginous (in blue) or ossified (in red) at the distal ends of hypurals 1 and 2, and the parhypural. Poisson regressions revealed a significant increase in distal radial number in *c13a* mutants ($\chi^2_{(2)}$=27.05, p<0.0001) but not significant in *b13a* mutants ($\chi^2_{(2)}$=1.98, p=0.37). Post-hoc comparisons showed a significant effect in $c13a^{-/-}$ mutants only. Scale bar is 100 µm. Each graph presents the mean, and the circle size is proportional to the number of individuals.

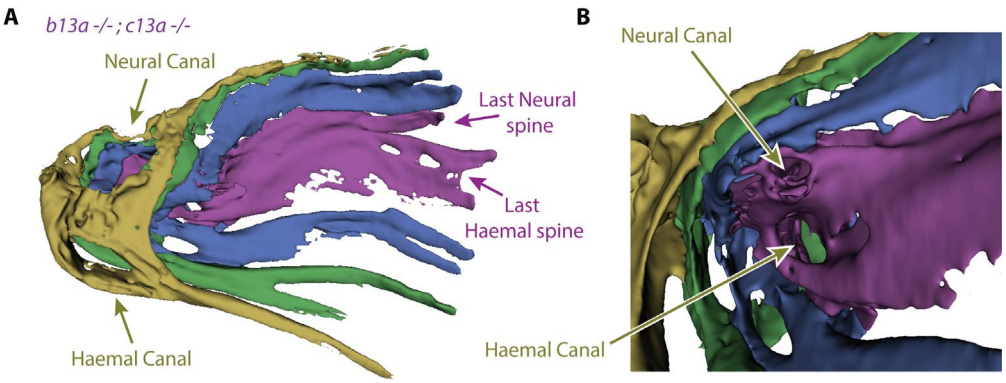

Fig. S8. Morphological and ontogenetic description of the posterior end of the tail of *b13a*$^{-/-}$;*c13a*$^{-/-}$ double mutant fish. (**A**), micro-CT segmentation of the last four vertebrae of an adult double mutant, showing extremely condensed and fused posterior elements. The last neural and haemal spines were partially fused together. (**B**), A close-up on the posterior end of the body axis reveals a neural and haemal canal all the way to the posterior-most element (purple), which implies the absence of hypurals and other ural elements.

Table S1. Gene IDs for each *hox13* gene present in a broad set of annotated genomes of actinopterygians. For each species, the family, assembly number, and the NCBI gene ID for each *hox* gene, if present, is given. A dash (–) indicates the absence of the corresponding gene in the respective gene cluster.

Species	Family	Assembly	*a13a*	*a13b*	*b13a*	*b13b*	*c13a*	*c13b*	*d13a*	*d13b*
Acanthopagrus latus	Sparidae	fAcaLat1.1 (GCF_904848185.1)	119016198	119006236	119014195	–	119022528	–	–	–
Alosa alosa	Clupeidae	AALO_Geno_1.1 (GCF_017589495.1)	–	125305489	125296091	–	125293421	125301534	125292652	–
Amphiprion ocellaris	Pomacentridae	AmpOce1.0 (GCF_002776465.1)	111570269	111588836	111568215	–	111581487	–	–	–
Anabas testudineus	Anabantidae	fAnaTes1.2 (GCF_900324465.2)	113153850	113170369	113160018	–	113167485	–	–	–
Anarrhichthys ocellatus	Anarhichadidae	GSC_Weel_1.0 (GCF_004355925.1)	116387229	116386823	116379203	–	116382332	–	–	–
Anguilla anguilla	Anguillidae	fAngAng1.pri (GCF_013347855.1)	118233193	118210810	118216130	–	118208357	118211264	118224185	–
Astyanax mexicanus	Characidae	AstMex3_surface (GCF_023375975.1)	103021373	125802465	103043948	–	103031462	125787537	103046722	–
Betta splendens	Osphronemidae	fBetSpl5.3 (GCF_900634795.3)	114865817	114843721	114860546	–	114858382	–	–	–
Brienomyrus brachyistius	Mormyridae	BBRACH_0.4 (GCF_023856365.1)	125719156	125749217	–	125742441	125713053	125723646	125710344	–
Chanos chanos	Chanidae	fChaCha1.1 (GCF_902362185.1)	115825775	115818678	115829565	–	115807888	115814502	115822611	–
Chelmon rostratus	Chaetodontidae	fCheRos1.pri (GCF_017976325.1)	121619703	121610632	121620985	–	121612905	–	–	–
Clupea harengus	Clupeidae	Ch_v2.0.2 (GCF_900700415.2)	–	105911402	105912847	–	105912700	105907699	105907975	–
Colossoma macropomum	Serrasalmidae	Colossoma_macropomum (GCF_904425465.1)	118805088	118813412	118821189	–	118822780	118800031	118805755	–
Cottoperca gobio	Bovichtidae	fCotGob3.1 (GCF_900634415.1)	115015782	115021485	115012486	–	115010850	–	–	–
Ctenopharyngodon idella	Xenocyprididae	HZGC01 (GCF_019924925.1)	127501065	127497339	127509312	–	127504894	127522540	127519347	–
Cynoglossus semilaevis	Cynoglossidae	Cse_v1.0 (GCF_000523025.1)	103394226	103388423	103393562	–	103385112	–	–	–
Cyprinodon tularosa	Cyprinodontidae	ASM1607723v1 (GCF_016077235.1)	119779531	119772787	119778601	–	119785041	–	–	–
Danio rerio	Cyprinidae	GRCz11 (GCF_000002035.6)	570239	30438	559921	–	58059	58063	30407	–
Denticeps clupeoides	Denticipitidae	fDenClu1.1 (GCF_900700375.1)	–	114789724	114793421	–	114798405	114800762	–	–
Electrophorus electricus	Gymnotidae	fEleEle1.pri (GCF_013358815.1)	113580414	113571216	113569906	–	113570296	113572414	113582335	–
Epinephelus fuscoguttatus	Serranidae	E.fuscoguttatus.final_Chr_v1 (GCF_011397635.1)	125904682	125893496	125879368	–	125891524	–	–	–
Erpetoichthys calabaricus	Polypteridae	fErpCal1.3 (GCF_900747795.2)	114664210	–	114664381		114647630	–	127528919	–
Esox lucius	Esocidae	fEsoLuc1.pri (GCF_011004845.1)	105023650	105018810	105013260	–	105013634	105016993	105016222	–
Fundulus heteroclitus	Fundulidae	MU-UCD_Fhet_4.1 (GCF_011125445.2)	105934282	105926310	–	–	105928933	–	–	–
Gadus morhua	Gadidae	gadMor3.0 (GCF_902167405.1)	115536261	115554199	115557907	–	115542510	–	–	–
Gambusia affinis	Poeciliidae	SWU_Gaff_1.0 (GCF_019740435.1)	122843743	122831439	122821262	–	122828352	–	–	–
Gasterosteus aculeatus	Gasterosteidae	GAculeatus_UGA_version5 (GCF_016920845.1)	120826906	120809982	120827242	–	120829913	–	–	–
Girardinichthys multiradiatus	Goodeidae	DD_fGirMul_XY1 (GCF_021462225.1)	124879185	124865511	124864643	–	124874917	–	–	–
Gouania willdenowi	Gobiesocidae	fGouWil2.1 (GCF_900634775.1)	114472436	114478105	114468953	–	114467248	–	–	–
Gymnodraco acuticeps	Bathydraconidae	fGymAcu1.1 (GCF_902827175.1)	117563002	117554052	117547479	–	117541974	–	–	–
Haplochromis burtoni	Cichlidae	NCSU_Asbu1 (GCF_018398535.1)	102313663	102305000	102307949	–	102309054	–	–	–
Hippocampus zosterae	Syngnathidae	ASM2543408v3 (GCF_025434085.1)	127603790	127601411	127590245	–	127596034	–	–	–
Hypomesus transpacificus	Osmeridae	fHypTra1 (GCF_021917145.1)	124467241	124479323	124479662	–	124481039	124471218	124484894	–

Ictalurus punctatus	Ictaluridae	IpCoco_1.2 (GCF_001660625.2)	108257341	100528527	108275712	–	124481039	108281070	108266222	–
Labeo rohita	Cyprinidae	IGBB_LRoh.1.0 (GCF_022985175.1)	127182171	127178305	127163141	–	127154533	127173481	127170654	–
Larimichthys crocea	Sciaenidae	L_crocea_2.0 (GCF_000972845.2)	104940566	104927762	104927154	–	113747701	–	–	–
Lates carcarifer	Latidae	TLL_Latcal_v3 (GCF_001640805.2)	108877307	108891462	108898525	–	108876406	–	–	–
Lepisosteus oculatus	Lepisosteidae	LepOcu1 (GCF_000242695.1)	102685955	–	102684356	–	102695065	–	102687373	–
Mastacembelus armatus	Mastacembelidae	fMasArm1.2 (GCF_900324485.2)	113126226	113122525	113141170	–	113145809	–	–	–
Megalops cyprinoides	Megalopidae	fMegCyp1.pri (GCF_013368585.1)	118796574	118784978	118794944	118786861	118781054	118779675	118788744	–
Melanotaenia boesemani	Melanotaeniidae	fMelBoe1.pri (GCF_017639745.1)	121657123	121641975	121630574	–	121651751	–	–	–
Micropterus dolomieu	Centrarchidae	ASM2129224v1 (GCF_021292245.1)	123976630	123968447	123963320	–	123974690	–	–	–
Monopterus albus	Synbranchidae	M_albus_1.0 (GCF_001952655.1)	109968138	109967340	109964752	–	109971443	–	–	–
Morone saxatilis	Moronidae	NCSU_SB_2.0 (GCF_004916995.1)	118342900	118336211	118322950	–	118324617	–	–	–
Mugil cephalus	Mugilidae	CIBA_Mcephalus_1.1 (GCF_022458985.1)	125020101	125016446	124997272	–	125004882	–	–	–
Myripristis murdjan	Holocentridae	fMyrMur1.1 (GCF_902150065.1)	115367737	115373564	115363531	–	115362656	–	–	–
Nothobranchius furzeri	Nothobranchiidae	Nfu_20140520 (GCF_001465895.1)	107383371	107373760	107372950	–	107390910	–	–	–
Notolabrus celidotus	Labridae	fNotCel1.pri (GCF_009762535.1)	117827578	117822401	117831858	–	117821136	–	–	–
Notothenia coriiceps	Nototheniidae	NC01 (GCF_000735185.1)	104941128	104949896	104961652	–	104956898	–	–	–
Oryzias latipes	Adrianichthyidae	ASM223467v1 (GCF_002234675.1)	101162380	101158301	101175240	–	101172814	–	–	–
Pangasianodon hypophthalmus	Pangasiidae	fPanHyp1.pri (GCF_027358585.1)	113536158	113542465	113527999	–	113530408	113537872	113526107	–
Parambassis ranga	Ambassidae	fParRan2.1 (GCF_900634625.1)	114450846	114448736	114440004	–	114438672	–	–	–
Paramormyrops kingsleyae	Mormyridae	PKINGS_0.1 (GCF_002872115.1)	111846880	111839073	–	111845174	111837113	111854629	111838605	–
Perca fluviatilis	Percidae	GENO_Pfluv_1.0 (GCF_010015445.1)	120570779	120562706	120573967	–	120558388	–	–	–
Periophthalmus magnuspinnatus	Gobiidae	fPerMag1.pri (GCF_009829125.1)	117378578	117384231	117374905	–	117373699	–	–	–
Pimephales promelas	Leuciscidae	EPA_FHM_2.0 (GCF_016745375.1)	120483476	120494977	120489151	–	120462838	120473470	120459864	–
Polyodon spathula	Polyodontidae	ASM1765450v1 (GCF_017654505.1)	121315113	–	121324053	–	121307103	–	121323563	–
Polypterus senegalus	Polypteridae	ASM1683550v1 (GCF_016835505.1)	120515966	–	120517882	–	120526741	–	120531872	–
Pseudochaenichthys georgianus	Channichthyidae	fPseGeo1.1 (GCF_902827115.1)	117455526	117461369	117451460	–	117449376	–	–	–
Puntigrus tetrazona	Cyprinidae	ASM1883169v1 (GCF_018831695.1)	122323997	122360656	122341821	–	122329075	122354330	122351297	–
Pygocentrus nattereri	Serrasalmidae	fPygNat1.pri (GCF_015220715.1)	108425156	108441525	108412326	–	108433367	108424576	108424277	–
Salarias fasciatus	Blenniidae	fSalaFa1.1 (GCF_902148845.1)	115380987	115396613	115387337	–	115408331	–	–	–
Salmo trutta A	Salmonidae	fSalTru1.1 (GCF_901001165.1)	115175456	115187781	115197040	–	115167868	115150489	115155476	–
Salmo trutta B	Salmonidae	fSalTru1.1 (GCF_901001165.1)	115173940	115187701	115171015	–	115165528	115207926	115160778	–
Scatophagus argus	Scatophagidae	fScaArg1.pri (GCF_020382885.2)	124074176	124064917	124073304	–	124063977	–	–	–
Scleropages formosus	Osteoglossidae	fSclFor1.1 (GCF_900964775.1)	108933365	108927390	108936910	108918676	108939194	108918377	–	–
Scophthalmus maximus	Scophthalmidae	ASM2237912v1 (GCF_022379125.1)	118292521	118302692	118288805	–	118316278	–	–	–
Sebastes umbrosus	Sebastidae	fSebUmb1.pri (GCF_015220745.1)	119503423	119496298	119501162	–	119489931	–	–	–
Seriola dumerili	Carangidae	Sdu_1.0 (GCF_002260705.1)	111223387	111238797	111669768	–	111219155	–	–	–
Silurus meridionalis	Siluridae	ASM1480568v1 (GCF_014805685.1)	124376121	124384259	124396948	–	124399096	124402352	124382995	–
Syngnathus acus	Syngnathidae	fSynAcu1.2 (GCF_901709675.1)	119130672	119136231	119126029	–	119119446	–	–	–

Tachysurus fulvidraco	Bagridae	HZAU_PFXX_2.0 (GCF_022655615.1)	113641606	113644199	113637995	–	113641954	113661989	113654529	–
Takifugu rubripes	Tetraodontidae	fTakRub1.2 (GCF_901000725.2)	101069611	101062469	101072102	–	101079732	–	–	–
Thalassophryne amazonica	Batrachoididae	fThaAma1.1 (GCF_902500255.1)	117501877	117514506	117527962	–	117511652	–	–	–
Thunnus albacares	Scombridae	fThuAlb1.1 (GCF_914725855.1)	122969662	122987517	122967155	–	122982087	–	–	–
Toxotes jaculatrix	Toxotidae	fToxJac2.pri (GCF_017976425.1)	121192022	121186135	121198671	–	121194472	–	–	–
Trematomus bernacchii	Nototheniidae	fTreBer1.1 (GCF_902827165.1)	117477647	117480696	117469296	–	117494396	–	–	–
Xiphias gladius	Xiphiidae	ASM1685928v1 (GCF_016859285.1)	120786631	120784448	120787991	–	120803580	–	–	–

Table S2. Character-taxon data matrix for the seven characters used in the character reconstruction analysis. State [–] represents the character is not applicable. Missing or ambiguous information is represented with [?]; †, extinct taxon.

Taxon	Characters						
	1	2	3	4	5	6	7
Amia calva	0	0	0	0	0	0	0
†*Amia pattersoni*	0	0	0	0	0	-	0
†*Anaethalion*	1	1	1	1	1	2	1
†*Ascalabos*	1	1	1	1	1	2	1
†*Aspidorhynchus*	1	0	1	0	1	1	0
†*Belonostomus*	1	0	1	0	1	0	0
†*Domeykos*	1	1	1	1	1	1	1
†*Dorsetichthys*	1	0	1	0	1	1	1
†*Ebertichthys*	1	1	-	1	1	2	1
Elops	1	1	1	0	1	2	1
†*Eurycormus*	1	0	1	0	1	1	1
Heterotis	1	–	0	1	0	0	1
Hiodon	1	1	1	1	0	1/2	1
†*Hypsocormus*	0	–	0	0	0	3	–
†*Leptolepis coryphaenoides*	1	1	1	1	1	2	0
Lepisosteus	0	0	0	0	0	0	0
†*Luisichthys*	?	1	1	0	1	-	1
†*Lycoptera*	1	0/1	1	1	0	0	1
Megalops	1	1	1	1	1	2	1
†*Obaichthys*	0	0	0	0	-	0	0
†*Orthocormus*	0	–	0	0	0	3	–
†*Pachycormus*	0	–	0	0	0	3	–
†*Parapholidophorus*	?	0	0	0	-	1	0

†*Pholidoctenus serianus*	1	0	0	0	1	0/3	0
†*Prohalecites*	1	0	0	0	1	0	0
†*Protoclupea*	1	1	1	0	1	1	1
†*Tharsis*	0/1	1	1	0	1	2	0
†*Varasichthys*	?	1	1	0	0	?	1
†*Vinctifer*	1	–	1	0	1	0	0

Table S3. Oligonucleotides for each of the experiments performed in this work. Oligonucleotides for *in situ* hybridization, single guide RNAs for CRISPR/Cas9 and genotyping primers for the heteroduplex mobility assay are detailed.

Identifier	Oligonucleotide
hoxa13a ISH probes	F: 5' AGGTAACTTCTCGCCAAGCC 3' R: 5' ATCCGTCTGCGTTTGTCCTT 3'
hoxb13a ISH probes	F: 5' GTTTGGTTGGAAGCGGCAAT 3' R: 5' GCTATGGCGCGGTGTTTTTA 3'
hoxc13a ISH probes:	F 5' GGTCCTGCATCCACGCTGG 3' R 5' CTGAGAGGTTGGTTGTCGCA 3'
hoxc13b ISH probes	F: 5' CTGGGCGGACACACTGATTT 3' R: 5' CTCGGAGAGACTCGTTGTGG 3'
hoxc12a ISH probes	F: 5' AATCCATCGGAGTCGTGCAA 3' R: 5' GGACAAAGCCTGTTCCCTCA 3'
sgRNA hoxb13a_1	5'_TAATACGACTCACTATA***GGCGTAGGGGATGGGACCTG***GTTTT AGAGCTAGAA_3'
sgRNA hoxb13a_2	5'_TAATACGACTCACTATA***GGGCCATGGACAAGGCTAGA***GTTTT AGAGCTAGAA_3'
sgRNA hoxc13a_1	5'_TAATACGACTCACTATA***GGGCAGCGCTTTGCCCACAG***GTTTT AGAGCTAGAA_3'
sgRNA hoxc13a_2	5'_TAATACGACTCACTATA***GGAGCGCTAGATGACGTCTG***GTTTT AGAGCTAGAA_3'
sgRNA 3' common primer:	5'_AAAAGCACCGACTCGGTGCCACTTTTTCAAGTTGATAACGG ACTAGCCTTATTTTAACTTGCTATTTCTAGCTCTAAAAC_3'
Heteroduplex mobility shift assay against *hoxb13a*	F: 5'_GGAATCTGATGGCCCACTCG_3' R: 5'_TCAGACGTGACCGGGGTATC_3'
Heteroduplex mobility shift assay against *hoxc13a*	F: 5'_GCAGCCCGTGATATGACG_3' R: 5'_CTGCAAGTTCACATTGTGCG_3'

Movie S1. Double mutant adult and larvae swimming. The movie shows the swimming behavior of double mutant adults alongside wild type fish to highlight the differences in caudal fin morphology. Notably, the fish in the video swim using their anal fin. Additionally, the movie includes footage of a juvenile fish during the tail coiling stage, showcasing their unique swimming behavior.

Movie S2. Micro-CT video of double *b13a*$^{-/-}$; *c13a*$^{-/-}$ mutant. Each vertebra is segmented in a different color.

REFERENCES AND NOTES

1. J. J. Heckel, Über das Wirbelsäulen-Ende bei Ganoiden und Teleostiern. *Sber. Akad. Wiss. Wien* **5**, 143–147 (1850).

2. A. Kölliker, *Über das Ende der Wirbelsäule der Ganoiden und einiger Teleostier*. (von Willhelm Engelmann, 1860).

3. J. A. Ryder, "On the origin of heterocercy and the evolution of the fins and fin rays of fishes," *Rep. US Comm. Fish and Fisheries*. (US Government Printing Office, 1884), pp. 981–1107.

4. H.-P. Schultze, G. Arratia, The composition of the caudal skeleton of teleosts (Actinopterygil: Osteichthyes). *Zool. J. Linn. Soc.* **97**, 189–231 (1989).

5. O. Nybelin, Zur Morphologie und Terminologie des Schwanzskelettes der Actinopterygier. *Ark. Zool.* **15**, 485–516 (1963).

6. B. D. Metscher, P. E. Ahlberg, "Origin of the teleost tail: Phylogenetic frameworks for developmental studies" in *Major Events in Early Vertebrate Evolution*, P. E. Ahlberg, Ed. (Taylor & Francis, 2001), chap. 19, pp. 333–349.

7. H.-P. Schultze, G. Arratia, "The caudal skeleton of basal teleosts, its conventions, and some of its major evolutionary novelties in a temporal dimension" in *Mesozoic Fishes 5 – Global Diversity and Evolution*, G. Arratia, H.-P. Schultze, M. V. H. Wilson, Eds. (Verlag Dr. Friedrich Pfeil, 2013), pp. 187–246.

8. G. Arratia, Complexities of early Teleostei and the evolution of particular morphological structures through time. *Copeia* **103**, 999–1025 (2015).

9. T. H. Huxley, Original communications: Observations on the development of some parts of the skeleton of fishes. *J. Cell Sci.* **1**, 33–46 (1859).

10. T. Desvignes, A. Carey, J. H. Postlethwait, Evolution of caudal fin ray development and caudal fin hypural diastema complex in spotted gar, teleosts, and other neopterygian fishes. *Dev. Dyn.* **247**, 832–853 (2018).

11. T. Desvignes, A. E. Robbins, A. Z. Carey, R. Bailon-Zambrano, J. T. Nichols, J. H. Postlethwait, K. Stankunas, Coordinated patterning of zebrafish caudal fin symmetry by a central and two peripheral organizers. *Dev. Dyn.* **251**, 1306–1321 (2022).

12. Y. Nakatani, P. Shingate, V. Ravi, N. E. Pillai, A. Prasad, A. McLysaght, B. Venkatesh, Reconstruction of proto-vertebrate, proto-cyclostome and proto-gnathostome genomes provides new insights into early vertebrate evolution. *Nat. Commun.* **12**, 4489 (2021).

13. O. Simakov, F. Marletaz, J. X. Yue, B. O'Connell, J. Jenkins, A. Brandt, R. Calef, C. H. Tung, T. K. Huang, J. Schmutz, N. Satoh, J. K. Yu, N. H. Putnam, R. E. Green, D. S. Rokhsar, Deeply conserved synteny resolves early events in vertebrate evolution. *Nat. Ecol. Evol.* **4**, 820–830 (2020).

14. E. B. Lewis, A gene complex controlling segmentation in *Drosophila*. *Nature* **276**, 565–570 (1978).

15. D. Duboule, P. Dollé, The structural and functional organization of the murine HOX gene family resembles that of *Drosophila* homeotic genes. *EMBO J.* **8**, 1497–1505 (1989).

16. S. J. Gaunt, R. Krumlauf, D. Duboule, Mouse homeo-genes within a subfamily, Hox-1.4, −2.6 and −5.1, display similar anteroposterior domains of expression in the embryo, but show stage- and tissue-dependent differences in their regulation. *Development* **107**, 131–141 (1989).

17. A. Graham, N. Papalopulu, R. Krumlauf, The murine and *Drosophila* homeobox gene complexes have common features of organization and expression. *Cell* **57**, 367–378 (1989).

18. N. Denans, T. Iimura, O. Pourquié, *Hox* genes control vertebrate body elongation by collinear Wnt repression. *eLife* **4**, e04379 (2015).

19. R. Aires, L. de Lemos, A. Novoa, A. D. Jurberg, B. Mascrez, D. Duboule, M. Mallo, Tail Bud progenitor activity relies on a network comprising *Gdf11*, *Lin28*, and *Hox13* genes. *Dev. Cell* **48**, 383–395.e8 (2019).

20. T. Young, J. E. Rowland, C. van de Ven, M. Bialecka, A. Novoa, M. Carapuco, J. van Nes, W. de Graaff, I. Duluc, J. N. Freund, F. Beck, M. Mallo, J. Deschamps, *Cdx* and *Hox* genes differentially regulate posterior axial growth in mammalian embryos. *Dev. Cell* **17**, 516–526 (2009).

21. K. D. Economides, L. Zeltser, M. R. Capecchi, *Hoxb13* mutations cause overgrowth of caudal spinal cordand tail vertebrae. *Dev. Biol.* **256**, 317–330 (2003).

22. A. R. Godwin, M. R. Capecchi, *Hoxc13* mutant mice lack external hair. *Genes Dev.* **12**, 11–20 (1998).

23. A. Amores, A. Force, Y L Yan, L. Joly, C. Amemiya, A. Fritz, R K Ho, J. Langeland, V. Prince, Y L Wang, M. Westerfield, M. Ekker, J. H. Postlethwait, Zebrafish hox Clusters and vertebrate genome evolution. *Science* **282**, 1711–1714 (1998).

24. D. Davesne, M. Friedman, A. D. Schmitt, V. Fernandez, G. Carnevale, P. E. Ahlberg, S. Sanchez, R. B. J. Benson, Fossilized cell structures identify an ancient origin for the teleost whole-genome duplication. *Proc. Natl. Acad. Sci. U.S.A.* **118**, e2101780118 (2021).

25. J. S. Taylor, I. Braasch, T. Frickey, A. Meyer, Y. Van de Peer, Genome duplication, a trait shared by 22000 species of ray-finned fish. *Genome Res.* **13**, 382–390 (2003).

26. R. Thummel, L. Li, C. Tanase, M. P. Sarras, Jr., A. R. Godwin, Differences in expression pattern and function between zebrafish *hoxc13* orthologs: Recruitment of Hoxc13b into an early embryonic role. *Dev. Biol.* **274**, 318–333 (2004).

27. M. Corredor-Adámez, M. Welten, H. Spaink, J. Jeffery, R. Schoon, M. De Bakker, C. Bagowski, A. Meijer, F. Verbeek, M. Richardson, Genomic annotation and transcriptome analysis of the zebrafish (*Danio* rerio) hoxcomplex with description of a novel member, hoxb13a. *Evol. Dev.* **7**, 362–375 (2005).

28. Z. Ye, D. Kimelman, Hox13 genes are required for mesoderm formation and axis elongation during early zebrafish development. *Development* **147**, dev185298 (2020).

29. J. Géraudie, V. Borday Birraux, Posterior *hoxa* genes expression during zebrafish bony fin ray development and regeneration suggests their involvement in scleroblast differentiation. *Dev. Genes Evol.* **213**, 182–186 (2003).

30. R. Thummel, M. Ju, M. P. Sarras, Jr., A. R. Godwin, Both *Hoxc13* orthologs are functionally important for zebrafish tail fin regeneration. *Dev. Genes Evol.* **217**, 413–420 (2007).

31. C. Fromental-Ramain, X. Warot, N. Messadecq, M. LeMeur, P. Dollé, P. Chambon, *Hoxa-13* and *Hoxd-13* play a crucial role in the patterning of the limb autopod. *Development* **122**, 2997–3011 (1996).

32. D. Ahn, R. K. Ho, Tri-phasic expression of posterior *Hox* genes during development of pectoral fins in zebrafish: Implications for the evolution of vertebrate paired appendages. *Dev. Biol.* **322**, 220–233 (2008).

33. R. Freitas, C. Gomez-Marin, J. M. Wilson, F. Casares, J. L. Gomez-Skarmeta, *Hoxd13* contribution to the evolution of vertebrate appendages. *Dev. Cell* **23**, 1219–1229 (2012).

34. T. Nakamura, A. R. Gehrke, J. Lemberg, J. Szymaszek, N. H. Shubin, Digits and fin rays share common developmental histories. *Nature* **537**, 225–228 (2016).

35. D. M. Parichy, M. R. Elizondo, M. G. Mills, T. N. Gordon, R. E. Engeszer, Normal table of postembryonic zebrafish development: Staging by externally visible anatomy of the living fish. *Dev. Dyn.* **238**, 2975–3015 (2009).

36. G. Arratia, Actinopterygian postcranial skeleton with special reference to the diversity of fin ray elements, and the problem of identifying homologies in *Mesozoic Fishes 4 – Homology and Phylogeny*, G. Arratia, H.-P. Schultze, M. V. H. Wilson, Eds. (Verlag Dr. Friedrich Pfeil, 2008), pp. 49–101.

37. N. C. Bird, P. M. Mabee, Developmental morphology of the axial skeleton of the zebrafish, *Danio rerio* (Ostariophysi: Cyprinidae). *Dev. Dyn.* **228**, 337–357 (2003).

38. H. Kryvi, K. Nordvik, P. G. Fjelldal, M. Eilertsen, J. V. Helvik, E. N. Storen, J. H. Long, Jr., Heads and tails: The notochord develops differently in the cranium and caudal fin of Atlantic Salmon (*Salmo salar,* L.). *Anat. Rec.* **304**, 1629–1649 (2021).

39. L. Lleras Forero, R. Narayanan, L. F. Huitema, M. VanBergen, A. Apschner, J. Peterson-Maduro, I. Logister, G. Valentin, L. G. Morelli, A. C. Oates, S. Schulte-Merker, Segmentation of the zebrafish axial skeleton relies on notochord sheath cells and not on the segmentation clock. *eLife* **7**, e33843 (2018).

40. N. Cumplido, M. L. Allende, G. Arratia, From Devo to Evo: Patterning, fusion and evolution of the zebrafish terminal vertebra. *Front. Zool.* **17**, 18 (2020).

41. D. Duboule, G. Morata, Colinearity and functional hierarchy among genes of the homeotic complexes. *Trends Genet.* **10**, 358–364 (1994).

42. C. Patterson, The caudal skeleton in lower Liassic pholidophorid fishes. *Bull.Br.Mus.Nat.Hist.Geol.* **16**, 201–239 (1968).

43. G. Arratia, "The caudal skeleton of Jurassic teleosts; a phylogenetic analysis" in *Early vertebrates and related problems in evolutionary biology*, M. Chang, H. Liu, G.-R. Zhang, Eds. (Science Press, 1991), pp. 249–340.

44. G. Arratia, New Triassic teleosts (Actinopterygii, Teleosteomorpha) from northern Italy and their phylogenetic relationships among the most basal teleosts. *J. Vertebr. Paleontol.* **37**, e1312690 (2017).

45. G. Arratia, Morphology, taxonomy, and phylogeny of Triassic pholidophorid fishes (Actinopterygii, Teleostei). *J. Vertebr. Paleontol.* **33**, 1–138 (2013).

46. G. Arratia, H. P. Schultze, H. Tischlinger, On a remarkable new species of *Tharsis*, a Late Jurassic teleostean fish from southern Germany: Its morphology and phylogenetic relationships. *Foss. Rec.* **22**, 1–23 (2019).

47. W. McGinnis, R. L. Garber, J. Wirz, A. Kuroiwa, W. J. Gehring, A homologous protein-coding sequence in *Drosophila* homeotic genes and its conservation in other metazoans. *Cell* **37**, 403–408 (1984).

48. E. B. Lewis, The bithorax complex: The first fifty years. *Int. J. Dev. Biol.* **42**, 403–415 (1998).

49. J. H. Postlethwait, H. A. Schneiderman, A clonal analysis of determination in *Antennapedia* a homoeotic mutant of *Drosophila melanogaster*. *Proc. Natl. Acad. Sci. U. S. A.* **64**, 176–183 (1969).

50. J. H. Postlethwait, H. A. Schneiderman, Pattern formation and determination in the antenna of the homoeotic mutant *Antennapedia* of *Drosophila melanogaster*. *Dev. Biol.* **25**, 606–640 (1971).

51. T. Sato, K. Kataoka, Y. Ito, S. Yokoyama, M. Inui, M. Mori, S. Takahashi, K. Akita, S. Takada, H. Ueno-Kudoh, H. Asahara, *Lin28a/let-7* pathway modulates the *Hox* code via *Polycomb* regulation during axial patterning in vertebrates. *eLife* **9**, e53608 (2020).

52. L. Thomson, L. Muresan, B. Steventon, The zebrafish presomitic mesoderm elongates through compaction-extension. *Cells Dev.* **168**, 203748 (2021).

53. A. Mongera, P. Rowghanian, H. J. Gustafson, E. Shelton, D. A. Kealhofer, E. K. Carn, F. Serwane, A. A. Lucio, J. Giammona, O. Campàs, A fluid-to-solid jamming transition underlies vertebrate body axis elongation. *Nature* **561**, 401–405 (2018).

54. L. Zhang, C. Kendrick, D. Julich, S. A. Holley, Cell cycle progression is required for zebrafish somite morphogenesis but not segmentation clock function. *Development* **135**, 2065–2070 (2008).

55. C. M. Bouldin, C. D. Snelson, G. H. Farr, D. Kimelman, Restricted expression of cdc25a in the tailbud is essential for formation of the zebrafish posterior body. *Genes Dev.* **28**, 384–395 (2014).

56. B. Steventon, F. Duarte, R. Lagadec, S. Mazan, J. F. Nicolas, E. Hirsinger, Species-specific contribution of volumetric growth and tissue convergence to posterior body elongation in vertebrates. *Development* **143**, 1732–1741 (2016).

57. R. T. Lee, J. P. Thiery, T. J. Carney, Dermal fin rays and scales derive from mesoderm, not neural crest. *Curr. Biol.* **23**, R336–R337 (2013).

58. C. Neutens, D. Adriaens, J. Christiaens, B. De Kegel, M. Dierick, R. Boistel, L. Van Hoorebeke, Grasping convergent evolution in syngnathids: A unique tale of tails. *J. Anat.* **224**, 710–723 (2014).

59. O. Larouche, M. L. Zelditch, R. Cloutier, A critical appraisal of appendage disparity and homology in fishes. *Fish Fish.* **20**, 1138–1175 (2019).

60. Y. Hadzhiev, Z. Lele, S. Schindler, S. W. Wilson, P. Ahlberg, U. Strahle, F. Muller, Hedgehog signaling patterns the outgrowth of unpaired skeletal appendages in zebrafish. *BMC Dev. Biol.* **7**, 75 (2007).

61. J. Letelier, E. de la Calle-Mustienes, J. Pieretti, S. Naranjo, I. Maeso, T. Nakamura, J. Pascual-Anaya, N. H. Shubin, I. Schneider, J. R. Martinez-Morales, J. L. Gomez-Skarmeta, A conserved Shh cis-regulatory module highlights a common developmental origin of unpaired and paired fins. *Nat. Genet.* **50**, 504–509 (2018).

62. R. Freitas, G. Zhang, M. J. Cohn, Evidence that mechanisms of fin development evolved in the midline of early vertebrates. *Nature* **442**, 1033–1037 (2006).

63. R. Freitas, G. J. Zhang, M. J. Cohn, Biphasic *Hoxd* gene expression in shark paired fins reveals an ancient origin of the distal limb domain. *PLOS ONE* **2**, e754 (2007).

64. A. Minelli, The origin and evolution of appendages. *Int. J. Dev. Biol.* **47**, 573–581 (2003).

65. A. Force, M. Lynch, F. B. Pickett, A. Amores, Y. L. Yan, J. Postlethwait, Preservation of duplicate genes by complementary, degenerative mutations. *Genetics* **151**, 1531–1545 (1999).

66. J. H. Postlethwait, I. G. Woods, P. Ngo-Hazelett, Y. L. Yan, P. D. Kelly, F. Chu, H. Huang, A. Hill-Force, W. S. Talbot, Zebrafish comparative genomics and the origins of vertebrate chromosomes. *Genome Res.* **10**, 1890–1902 (2000).

67. C. T. Hittinger, S. B. Carroll, Gene duplication and the adaptive evolution of a classic genetic switch. *Nature* **449**, 677–681 (2007).

68. D. L. Stern, The genetic causes of convergent evolution. *Nat. Rev. Genet.* **14**, 751–764 (2013).

69. L. Chen, A. L. DeVries, C. H. Cheng, Convergent evolution of antifreeze glycoproteins in Antarctic notothenioid fish and Arctic cod. *Proc. Natl. Acad. Sci. U.S.A.* **94**, 3817–3822 (1997).

70. D. L. Stern, V. Orgogozo, The loci of evolution: How predictable is genetic evolution? *Evolution* **62**, 2155–2177 (2008).

71. L. Grande, W. E. Bemis, A comprehensive phylogenetic study of amiid fishes (Amiidae) based on comparative skeletal anatomy. an empirical search for interconnected patterns of natural history. *J. Vertebr. Paleontol.* **18**, 1–696 (1998).

72. T. Desvignes, A. Carey, I. Braasch, T. Enright, J. H. Postlethwait, Skeletal development in the heterocercal caudal fin of spotted gar (*Lepisosteus oculatus*) and other lepisosteiformes. *Dev. Dyn.* **247**, 724–740 (2018).

73. H. P. Schultze, G. Arratia, Reevaluation of the caudal skeleton of some actinopterygian fishes: II. Hiodon, Elops, and Albula. *J. Morphol.* **195**, 257–303 (1988).

74. G. Arratia, H.-P. Schultze, Reevaluation of the caudal skeleton of certain actinopterygian fishes: III. Salmonidae. Homologization of caudal skeletal structures. *J. Morphol.* **214**, 187–249 (1992).

75. E. J. Hilton, R. Britz, "The caudal skeleton of osteoglossomorph fishes, revisited: Comparisons, homologies, and characters" in *Origin and Phylogenetic Interrelationships of*

Teleosts, J. S. Nelson, H.-P. Schultze, M. V. H. Wilson, Eds. (Verlag Dr. Friedrich Pfeil, 2010), pp. 219–237.

76. D. F. Vaz, E. J. Hilton, The caudal skeleton of batrachoidiformes (Teleostei: Percomorphacea): A study of morphological diversity, intraspecific variation, and phylogenetic inferences. *Zool. J. Linn. Soc.* **189**, 228–286 (2020).

77. P. Thieme, P. Warth, T. Moritz, Development of the caudal-fin skeleton reveals multiple convergent fusions within Atherinomorpha. *Front. Zool.* **18**, 20 (2021).

78. W. A. Gosline, Some osteological features of modern lower teleostean fishes. *Smithson. Misc. Collect. Washingt.* **142**, 1–42 (1961).

79. K. Hoshino, Homologies of the caudal fin rays of Pleuronectiformes (Teleostei). *Ichthyol. Res.* **48**, 231–246 (2001).

80. M. Westerfield, *The zebrafish book: A guide for the laboratory use of zebrafish* (*Danio rerio*). (Univ. of Oregon Press, ed. 4th, 2000).

81. C. B. Kimmel, W. W. Ballard, S. R. Kimmel, B. Ullmann, T. F. Schilling, Stages of embryonic development of the zebrafish. *Dev. Dyn.* **203**, 253–310 (1995).

82. E. O. Wiley, A. M. Fuiten, M. H. Doosey, B. K. Lohman, C. Merkes, M. Azuma, The caudal skeleton of the zebrafish, *Danio rerio*, from a phylogenetic perspective: A polyural interpretation of homologous structures. *Copeia* **103**, 740–750 (2015).

83. A. Bensimon-Brito, M. L. Cancela, A. Huysseune, P. E. Witten, The zebrafish (*Danio rerio*) caudal complex - a model to study vertebral body fusion. *J. Appl. Ichthyol.* **26**, 235–238 (2010).

84. H. Acloque, D. G. Wilkinson, M. A. Nieto, "Chapter 9 In Situ Hybridization Analysis of Chick Embryos in Whole-Mount and Tissue Sections" in *Avian Embryology, 2nd Edition*. (2008), pp. 169–185.

85. A. Muto, S. Ikeda, M. E. Lopez-Burks, Y. Kikuchi, A. L. Calof, A. D. Lander, T. F. Schilling, Nipbl and mediator cooperatively regulate gene expression to control limb development. *PLOS Genet.* **10**, e1004671 (2014).

86. C. Thisse, B. Thisse, High-resolution in situ hybridization to whole-mount zebrafish embryos. *Nat. Protoc.* **3**, 59–69 (2008).

87. A. Hruscha, P. Krawitz, A. Rechenberg, V. Heinrich, J. Hecht, C. Haass, B. Schmid, Efficient CRISPR/Cas9 genome editing with low off-target effects in zebrafish. *Development* **140**, 4982–4987 (2013).

88. W. Y. Hwang, Y. Fu, D. Reyon, M. L. Maeder, S. Q. Tsai, J. D. Sander, R. T. Peterson, J. R. Yeh, J. K. Joung, Efficient genome editing in zebrafish using a CRISPR-Cas system. *Nat. Biotechnol.* **31**, 227–229 (2013).

89. L. E. Jao, S. R. Wente, W. Chen, Efficient multiplex biallelic zebrafish genome editing using a CRISPR nuclease system. *Proc. Natl. Acad. Sci. U.S.A.* **110**, 13904–13909 (2013).

90. M. A. Moreno-Mateos, C. E. Vejnar, J.-D. Beaudoin, J. P. Fernandez, E. K. Mis, M. K. Khokha, A. J. Giraldez, CRISPRscan: Designing highly efficient sgRNAs for CRISPR-Cas9 targeting in vivo. *Nat. Methods* **12**, 982–988 (2015).

91. T. Nakayama, I. L. Blitz, M. B. Fish, A. O. Odeleye, S. Manohar, K. W. Cho, R. M. Grainger, Cas9-based genome editing in *Xenopus tropicalis*. *Method. Enzymol.* **546**, 355–375 (2014).

92. S. Ansai, M. Kinoshita, Targeted mutagenesis using CRISPR/Cas system in medaka. *Biol. Open* **3**, 362–371 (2014).

93. E. L. Sorlien, M. A. Witucki, J. Ogas, Efficient production and identification of CRISPR/Cas9-generated gene knockouts in the model system *Danio rerio*. *J. Vis. Exp.*, e56969 (2018).

94. M. B. Walker, C. B. Kimmel, A two-color acid-free cartilage and bone stain for zebrafish larvae. *Biotech. Histochem.* **82**, 23–28 (2007).

95. E. H. Bryant, On use of logarithms to accommodate scale. *Syst. Zool.* **35**, 552–559 (1986).

96. P. Sordino, D. Duboule, T. Kondo, Zebrafish *Hoxa* and *Evx-2* genes: Cloning, developmental expression and implications for the functional evolution of posterior *Hox* genes. *Mech. Dev.* **59**, 165–175 (1996).

97. C. Thisse, B. Thisse, High throughput expression analysis of ZF-models consortium clones. *ZFIN Direct Data Submission.* (2005).

98. C. Patterson, "The contribution of paleontology to teleostean phylogeny" in *Major Patterns in Vertebrate Evolution*, M. K. Hecht, P. C. Goody, B. M. Hecht, Eds. (Plenum, 1977), vol. **14**, pp. 579–643.

99. P. M. Brito, Révision des Aspidorhynchidae (Pisces, Actinopterygii) du Mésozoïque: Ostéologie, relations phylogénétiques, données environnementales et biogéographiques. *Geodiversitas* **19**, 681–772 (1997).

100. H.-P. Schultze, G. Arratia, Reevaluation of the caudal skeleton of actinopterygian fishes: I. Lepisosteus and Amia. *J. Morphol.* **190**, 215–241 (1986).

101. G. Arratia, "The monophyly of Teleostei and stem-group teleosts" in *Mesozoic Fishes 2 – Systematics and Fossil Record*, G. Arratia, H.-P. Schultze, Eds. (Dr. Friedrich Pfeil, München, 1999), vol. 2, pp. 265–334.

102. G. Arratia, Basal teleosts and teleostean phylogeny. *Paleo Ichth.* **7**, 5–168 (1997).

103. G. Arratia, Remarkable teleostean fishes from the Late Jurassic of southern Germany and their phylogenetic relationships. *Mitt. Mus. Nat. Kd., Berl. Geowiss. Reihe* **3**, 137–179 (2000).

104. C. Patterson, D. E. Rosen, Review of ichthyodectiform and other Mesozoic teleost fishes, and the theory and practice of classifying fossils. *Bull. Am. Mus. Nat. Hist.* **158**, 81–172 (1977).

105. R. R. Betancur, E. O. Wiley, G. Arratia, A. Acero, N. Bailly, M. Miya, G. Lecointre, G. Orti, Phylogenetic classification of bony fishes. *BMC Evol. Biol.* **17**, 162 (2017).

106. E. Parey, A. Louis, J. Montfort, O. Bouchez, C. Roques, C. Iampietro, J. Lluch, A. Castinel, C. Donnadieu, T. Desvignes, C. Floi Bucao, E. Jouanno, M. Wen, S. Mejri, R. Dirks, H. Jansen, C. Henkel, W. J. Chen, M. Zahm, C. Cabau, C. Klopp, A. W. Thompson, M. Robinson-Rechavi, I. Braasch, G. Lecointre, J. Bobe, J. H. Postlethwait, C. Berthelot, H. R. Crollius, Y. Guiguen, Genome structures resolve the early diversification of teleost fishes. *Science* **379**, 572–575 (2023).